Kinetics, selectivity and scale up of the Fischer-Tropsch synthesis

van der Laan, Gerard Pieter

6

Kinetics and Selectivity of the Gas-Slurry Fischer-Tropsch Synthesis

Abstract

The kinetics of the Fischer-Tropsch (FT) synthesis over a commercial Fe-Cu-K-SiO_2 catalyst was studied in a continuous gas-slurry reactor. A novel product distribution model, recently developed to describe the product selectivity of a gas-solid FT synthesis was applied to model the product distributions obtained at industrially relevant conditions (reactor pressure of 1.2-4.0 MPa, H_2/CO feed ratio of 0.25-4.0, space velocity of 0.25-0.77 10^{-3} Nm^3 kg_{cat}^{-1} s^{-1}, and a constant temperature of 523 K) over a precipitated iron catalyst in the slurry phase. The new model, called Olefin Readsorption Product Distribution Model (ORPDM), combines a mechanistic model of olefin readsorption with kinetics of chain growth and termination on the same catalytic sites. In the slurry phase, this model appears to describe the deviations from the classical Anderson-Schulz-Flory distribution accurately. The selectivity to paraffins and olefins could be predicted with average deviations of 10.6 % and 8.7 %, respectively. The presence of the slurry liquid appeared to affect both the model parameters and the product selectivity relative to the gas-solid kinetics. The slurry-phase system shows a higher olefin content at comparable reaction conditions. The corresponding model parameters, the readsorption constant and the termination constant to olefins, are all lower at similar process conditions than the corresponding model parameters for the gas-solid kinetics. The intrinsic kinetics is also influenced by the slurry liquid. At H_2/CO ratios < 2, both the Fischer-Tropsch and the water gas shift reaction rates are lower than for the gas-solid system. The slurry liquid influences the adsorption of CO_2 on FT sites and causes a complete coverage of the water gas shift sites.

6.1 Introduction

The Fischer-Tropsch (FT) synthesis converts synthesis gas into a multicomponent mixture of predominantly hydrocarbons. The Fischer-Tropsch synthesis in slurry bubble columns is very attractive relative to fixed bed reactors [1]. The advantages are: 1) Low pressure drop over the reactor. 2) Excellent heat transfer characteristics resulting in stable reactor temperatures. 3) No diffusion limitations. 4) Possibility of continuous refreshment of catalyst particles. 5) Relatively simple construction and low investment costs.

Recently, we developed a novel product selectivity model for linear paraffins and α-olefins (see Chapter 4). The α-Olefin Readsorption Product Distribution Model (ORPDM) accounts for secondary readsorption of α-olefins on FT growth sites on the precipitated iron catalyst. The proposed reaction network is shown in Figure 4.1. The readsorption rates of the olefins are supposed to increase exponentially with carbon number due to the increase of both physisorption effects and solubility with increasing chain length. ORPDM accounts for chain-length dependent readsorption of olefins on FT sites. The readsorption step depends on carbon number, resulting in a net decrease of the termination probability to olefins. α_n increases with increasing chain length until no olefins are formed anymore. At high carbon numbers, the chain growth parameter, α_n, approaches a maximum constant value. The increased readsorption of long-chain olefins results in a decreasing olefin/paraffin ratio with increasing chain length.

Intrinsic rate expressions for the Fischer-Tropsch (FT) reaction and the water gas shift (WGS) reaction on the same precipitated iron catalyst in a gas-solid system are reported in Chapter 5. These kinetic equations are based on the Langmuir-Hinshelwood-Hougen-Watson and the Eley-Rideal approach using a detailed scheme of potentially possible reaction mechanisms. The same set of kinetic equations will be tested for the description of the gas-slurry kinetics. The liquid-phase may influence heterogeneous reaction kinetics (Van der Laan et al. [2]):

1. The rate of reaction may be significantly affected by introducing any non-"ideal" (interacting) liquids.

2. Competitive adsorption of a slurry liquid on active catalytic sites will reduce the reaction rates.

3. The slurry liquid can interact with weakly adsorbed surface species.

4. Differences in solubility of reactants and products in various solvents explains the difference in liquid-phase concentration.

Several studies concerning both the Fischer-Tropsch, the methanol, and the methanol-higher alcohol synthesis are of special interest. Stenger and Satterfield [3, 4] measured the effect of the nature of an inert liquid on the reaction rate and on the selectivity of the Fischer-Tropsch synthesis on a reduced fused magnetite catalyst. They observed that the reaction rate of the Fischer-Tropsch synthesis in presence of phenantrene is nearly twice as fast as in n-octacosane and triphenylmethane, even though the solubility is slightly lower in phenantrene. The presence of phenantrene caused reduction of deposit formation (catalyst deactivation) and readsorption of primary olefins onto the catalyst and hence inhibited secondary reactions. Bukur et al. [5] measured the activity and selectivity of a Ruhrchemie LP 33/81 catalyst both in gas-solid (tubular fixed bed) and in slurry systems. The initial activity and selectivity was about the same for both systems. However, catalyst aging affected the hydrocarbon distribution differently. In the slurry system the olefin selectivity decreased, while the internal olefins and oxygenated production rates increased with time on stream, whereas the opposite changes were observed in the gas-solid system. Bukur et al. [5] reported similar effects of changes in the process conditions (temperature, pressure, H_2/CO feed ratio and space velocity) on the product selectivities. The initial FT activity was the same in both systems, whereas the WGS selectivity (carbon dioxide production relative to the carbon monoxide consumption) was somewhat higher in gas-solid system [5].

Graaf et al. [6] observed a significant contribution of the methanol formation via CO_2 by introducing squalane as a solvent, relative to the two-phase system. The three-phase methanol synthesis in squalane is much less sensitive to the temperature. Van der Laan et al. [2] measured the kinetics of the three-phase methanol synthesis both in an apolar solvent, squalane, and in a polar solvent, tetra ethylene glycol dimethylether (TEGDME). The slurry liquid appears to affect both the activation energy and the kinetic rate constant by interactions between adsorbed species and solvent and by competitive adsorption of the solvent on the catalyst surface. The rate of reaction to methanol observed in TEGDME appeared to be 10 times lower than in squalane.

The kinetics of both the gas-solid and gas-slurry (n-octacosane) methanol-higher alcohol synthesis from $CO/CO_2/H_2$ was investigated by Breman et al. [7]. The presence of n-octacosane as a slurry liquid appeared to affect the product distributions and the activity of the catalyst relative to the gas-solid system: lower $CO+CO_2$ reaction rates, lower higher alcohol to methanol selectivities, higher hydrocarbon yields, and lower water gas shift reaction rates.

The aim of this study is to test the Olefin Readsorption Product Distribution Model,

recently developed for the gas-solid system, for predicting gas-slurry product distributions at industrially relevant conditions on a precipitated iron catalyst. The gas-slurry kinetics will be modeled starting from a comprehensive set of equations proposed elsewhere (Chapter 5). Furthermore, the effects of process conditions on the kinetics and the selectivity of the gas-slurry Fischer-Tropsch synthesis are investigated experimentally and the results are compared with the performance of a gas-solid system.

6.2 Experimental

6.2.1 Slurry Reactor

The Fischer-Tropsch experiments were carried out in a gas-continuous slurry reactor. A detailed description of the experimental setup and analysis sections is given in Chapter 3. The slurry reactor is a 1.8 dm^3 autoclave (H= 18.2 cm, D= 12.0 cm) made by Medimex (see Figure 3.3). During the Fischer-Tropsch reaction, liquid products can be formed. The level of the slurry was maintained constant using a home-made filtering unit. The liquid products were removed via a filter (sintered metal 5 μm), whereas the catalyst particles remained inside the reactor. The liquid and gas phase volumes applied were 730 and 985 cm^3, respectively.

6.2.2 Experimental Procedure

The slurry reactor was loaded with 7.3 g of unreduced catalyst particles with 40 $\leq d_P \leq$ 50 μm. The catalyst applied was a commercial precipitated iron catalyst (type LP 33/81) synthesized by Ruhrchemie AG (Oberhausen, Germany). Details of this catalyst are given in Chapter 3. The catalyst was pretreated with hydrogen at a flow rate of 0.83 10^{-3} Nm^3 kg_{cat}^{-1} s^{-1} according to Bukur et al. [8]. The gas space velocity was based on the total mass of the unreduced supported catalyst. The reactor temperature, T, was increased linearly from 293 K to 553 K by 0.017 K s^{-1}. T remained at 553 K for 24 hours at an increased pressure of 1.0 MPa to prevent excessive solvent evaporation. After reduction, synthesis gas was fed to the reactor at reference conditions of 523 K, 1.50 MPa, F= 0.67 and a space velocity of 0.25 10^{-3} Nm^3 kg_{cat}^{-1} s^{-1}.

Liquid products were accumulated in high and low-pressure condensers for a typical period of 8-12 hours during steady state of the reactor system. The products were collected and weight before analysis. Several on-line GC analysis were performed during this period. Mass and atomic balances were typically 100 $\pm$ 10 %. After changing

the process conditions the reactor operated at least 48 hours undisturbed before a new mass balance period was started.

The variation of the experimental conditions at a constant temperature of 523 K are given in Chapter 3. The reference experiment was repeated 6 times to determine possible deactivation effects on the activity and selectivity of the catalyst. A summary of relevant experimental data is given in Appendix B. 27 kinetic experiments were carried out in the slurry reactor with the Ruhrchemie precipitated iron catalyst at 523 K in two separate catalyst tests, series B and series C.

6.3 Results and Discussion

6.3.1 Product Distribution Modeling

The olefin readsorption product distribution model (ORPDM) was tested to our experiments at 523 K. The model parameters were optimized for each experiment with the Levenberg-Marquardt method [9]. The number of parameters in model ORPDM was equal to 7: $p, t_O, k_R, c, t_P^1, t_P^2$, and k_R^2. Similar to a previous study (Chapter 4), the number of optimized parameters could be reduced because four parameters appeared to be independent of the experimental conditions. The average values of these parameters are shown in Table 6.1. For comparison, the corresponding values for the gas-solid study (Chapter 4) are also given in this table. Introduction of these mean model parameters at 523 K for both the increased readsorption of ethene relative to other olefins ($k_R^2/k_R e^{2\,c}$) and for the termination to C_1 (t_P^1) and C_2 products (t_P^2) and the exponential increase of the readsorption rate (c) reduces the number of parameters to be optimized from 7 to 3 within each experiment. Remarkably, both the readsorption rate of ethene and the exponential factor c are higher in both gas-slurry experimental series than observed for the gas-solid system.

Table 6.1 Optimized model parameters for ORPDM at 523 K that are independent of $\Phi_{v,0}$, P, H_2/CO ratio.

model parameter	G-S (A)	G-L-S (B)	G-L-S (C)
t_P^1	6.6	5.4	6.5
t_P^2	1.6	1.3	1.7
$k_R^2/k_R e^{2\,c}$	12.6	25.4	17.6
c	0.29	0.36	0.35

Table 6.2 Optimized model parameters ORPDM.

Run	p	t_O	k_R	n	s_{rel}	Run	p	t_O	k_R	n	s_{rel}
B1	17.92	6.39	0.037	19	8.9	C1	11.42	4.25	0.112	17	11.7
B2	14.08	6.59	0.063	19	16.4	C2	12.69	3.34	0.047	18	12.8
B3	12.04	5.63	0.075	19	10.8	C3	9.38	4.22	0.301	19	14.0
B4	15.90	5.25	0.040	18	13.5	C4	5.43	4.52[1]	-	19	19.9
B5	8.17	3.62	0.197	18	13.9	C5	12.62	4.12	0.098	19	12.2
B6	7.27	2.92	0.247	19	9.1	C6	11.83	4.65	0.119	18	13.0
B7	14.22	4.71	0.059	19	8.3	C7	21.48	7.05	0.087	19	12.3
B8	15.20	5.49	0.030	18	20.3	C8	9.55	5.90	0.339	19	14.8
B9	15.46	5.48	0.026	19	11.8	C9	7.28	7.26	0.869	19	18.0
B10	19.55	6.47	0.020	19	11.0	C10	14.54	5.15	0.070	16	14.7
B11	8.86	2.95	0.110	17	18.5	C11	23.12	7.62	0.085	18	11.9
B12	13.60	4.76	0.038	19	16.1	C12	17.05	6.32	0.113	19	8.7
						C13	5.99	5.70	0.631	19	17.8
						C14	16.33	8.47	0.056	16	17.7
						C15	19.26	7.28	0.056	15	7.9

[1] t_O/k_R

The three remaining model parameters (p, t_O, k_R) to be optimized within each experiment and the number of selectivities and s_{rel} for both experimental gas-slurry series B and C are given in Table 6.2. Table 6.3 shows the accuracies of the optimized models expressed with the relative standard deviation s_{rel} and the $MARR$ function for the paraffins and olefins, respectively, both for the gas-solid as well as the gas-slurry experiments at 523 K. The total number of selectivities n as well as the total number of optimized parameters m within a catalyst test are also included in this table. Figure 6.1a-b shows that the relative residuals between model ORPDM and experiments are almost always within 25 % in both catalyst tests.

Table 6.3 Accuracies of the Olefin Readsorption Product Distribution Models.

model	$MARR$ %		s_{rel} %	n	m
	paraffins	olefins			
G-S (A)	10.1	9.1	13.3	370	57
G-L-S (B)	9.4	8.4	12.5	223	36
G-L-S (C)	11.8	9.0	14.0	270	44

The model parameters of model ORPDM are pseudo kinetic rate constants, incorporating true kinetic rate constants, surface concentrations of intermediates, hydrogen

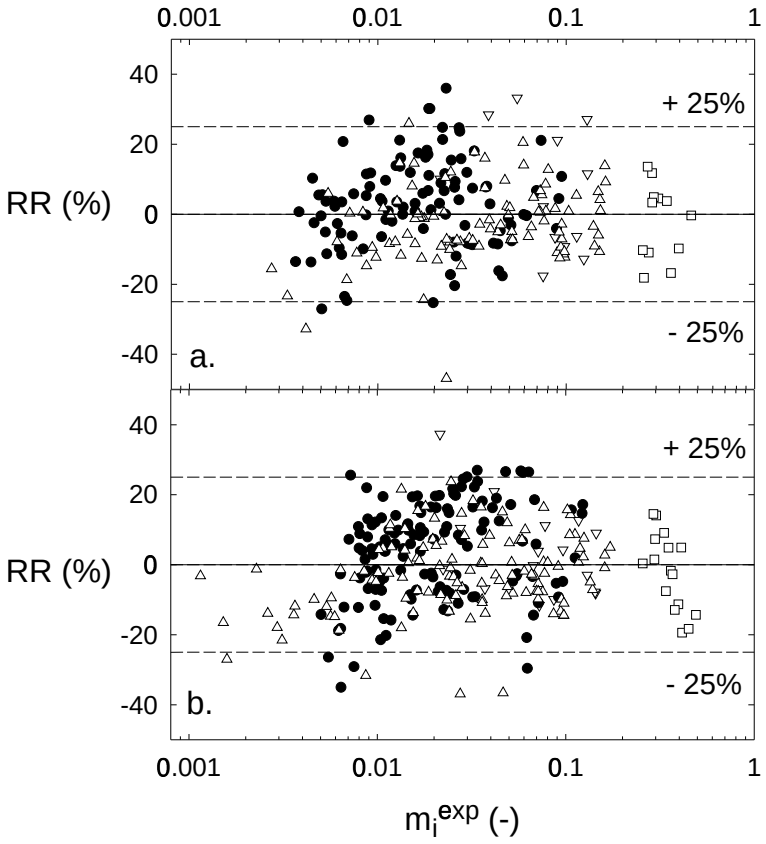

Figure 6.1 Relative residuals versus experimental selectivities. (•: paraffins, □: methane, △: olefins, ▽: ethene) Model ORPDM. a. Gas-slurry series B; b. Gas-slurry series C.

and vacant sites. Therefore, the model parameters vary with the adjusted process variables, P_{CO}, P_{H_2}, and space velocity. The effect of the process variables on the model parameters (p, t_O, k_R) was described with the same equations as in Table 6.4 (Chapter 4). The readsorption parameter, k_R, increases with H_2 pressure and decreases with CO pressure. CO inhibits readsorption rates, while a high H_2/CO ratio is favorable for readsorption of olefins. The accuracy of the equations presented in Table 6.4 is shown in Figure 6.2. Remarkably, the readsorption constant (k_R) and the termination constant to olefins (t_O) appear to be lower at similar process conditions than the corresponding model parameters for the gas-solid system. Both effects will result in a higher predicted olefin selectivity for the gas-slurry reactor.

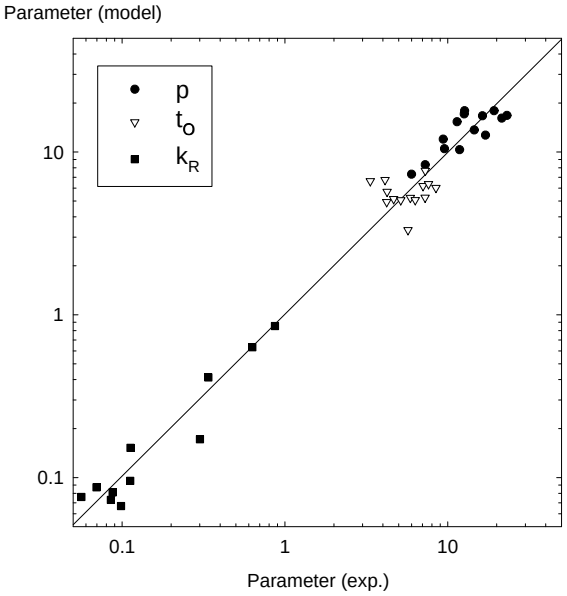

Figure 6.2 Parity graph of experimental (Table 6.2) and modeled parameters (Table 6.4) of model ORPDM.

Table 6.4 Model parameters ORPDM at 523 K in gas-solid (Chapter 4) and gas-slurry (C) experiments.

Parameter	G-S (A)	G-L-S (C)
p	$13.8 P_{H_2}^{-0.47} P_{CO}^{0.43}$	$14.4 P_{H_2}^{-0.26} P_{CO}^{0.40}$
t_O	$6.17 P_{H_2}^{-0.5}$	$3.71 P_{H_2}^{-0.5}$
k_R	$3.32\ 10^{-4} \frac{P_{H_2}^{1.4} P_{CO}^{-0.49}}{\Phi_{v,0}/W}$	$8.00\ 10^{-5} \frac{P_{H_2}^{1.2} P_{CO}^{-0.47}}{\Phi_{v,0}/W}$

ORPDM describes n-dependent readsorption of olefins, resulting in a curved distribution of paraffins and a decreasing O/P ratio with carbon number. Examples of product distributions with the predicted model values from model ORPDM are shown in Figure 6.3a-b and Table 6.5. The modeled product distributions appeared to predict the experimentally observed selectivities accurately. The deviations for C_1 and C_2

products, as well as the increasing paraffin content of the products are also described accurately. These figures also compare product distributions between two experiments from this study and gas-solid system experiments at comparable conditions (Chapter 4). Figure 6.3a-b and Table 6.5 show that the slurry liquid influences the product distribution obtained. It should be noted that the experimental conditions inside the reactor are not completely similar. The olefin content of the hydrocarbon mixture is higher in both gas-slurry experiments as a result of the model parameters (see Table 6.5 for p, t_O, and k_R). In accordance with Stenger and Satterfield [4], the readsorption of olefins is reduced in presence of the slurry liquid resulting in an increase of the olefin selectivity. In both comparisons, the selectivity to olefins is higher in the gas-slurry reactor. The selectivity to low molecular weight hydrocarbons appears to be decreased in the slurry system relative to the gas-solid system.

Table 6.5 Model parameters ORPDM, experimental conditions and selectivities (wt%) for Figure 6.3.

	Figure 6.3a		Figure 6.3b	
	Gas-solid	Gas-slurry	Gas-solid	Gas-slurry
Run	A16	B8	A8	B11
F	0.5	0.5	2.0	2.0
H_2/CO	0.38	0.30	6.19	4.71
$\Phi_{v,0}/W$ (10^{-3} Nm^3 kg$_{cat}$s^{-1})	0.36	0.39	0.35	0.34
p	19.46	15.20	6.69	8.86
t_O	5.50	5.49	4.22[1]	2.95
k_R	0.076	0.030	-	0.110
w_1	9.0	8.4	16.6	12.8
w_{2-4}	36.6	41.3	34.4	37.6
w_{5-10}	48.8	50.2	34.9	49.6
$w_{O,2-4}$	75.3	80.9	45.5	58.6
$w_{O,5-10}$	72.9	75.0	35.0	57.1

[1] t_O/k_R

6.3.2 Reaction Kinetics

The reaction rates of the Fischer-Tropsch synthesis (R_{FT}) and the water gas shift reaction (R_{WGS}) were calculated from the experimental results of experimental series C in Appendix B. The kinetic models applied were optimized for series C. The set of

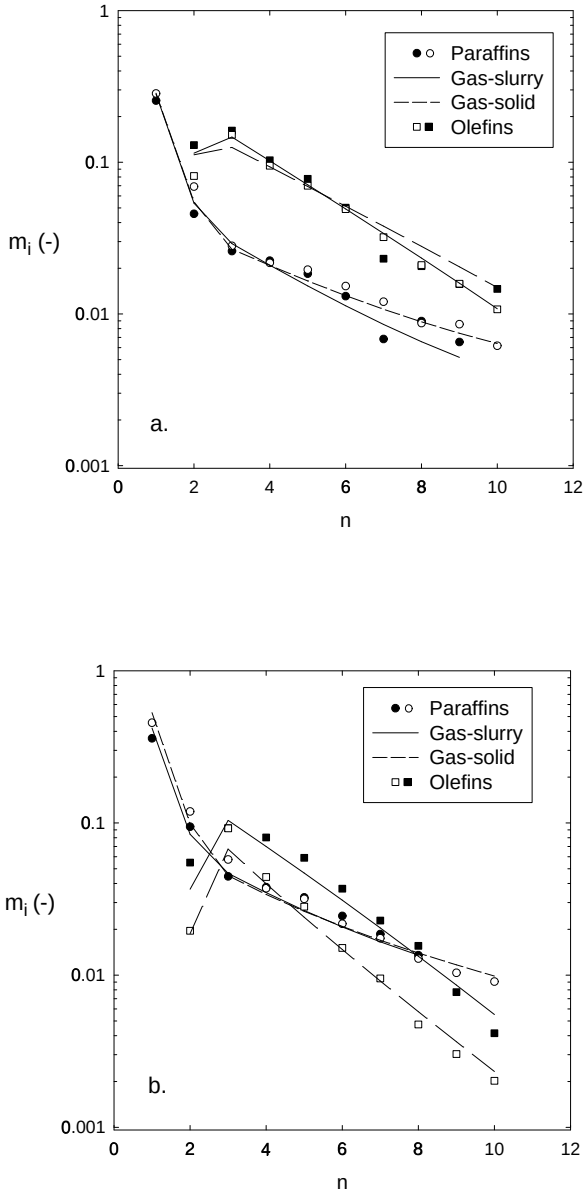

Figure 6.3 Product distributions as a function of carbon number for both the gas-slurry system (solid symbols, solid lines) and the gas-solid study (Chapter 4) (open symbols, dashed lines). Symbols are experimental selectivities. Lines are model predictions from ORPDM. Optimized parameters and the experimental conditions are shown in Table 6.5.

rate expressions developed in Chapter 5 were used for kinetic modeling in this study. These Langmuir-Hinshelwood-Hougen-Watson type of intrinsic rate expressions were derived on the basis of a detailed set of reaction mechanisms for the hydrocarbon formation as well as for the water gas shift equation. The same set of assumptions given in Chapter 5 was used for the development of the kinetic equations. In addition, however, it was assumed that carbon dioxide adsorbed strongly on the catalytic sites active for the Fischer-Tropsch reaction whereas the adsorption of water was assumed to be negligible. This, because of the experimental observations of high carbon dioxide concentrations in the reactor effluent (see Appendix B, series C) relative to water. Kinetic equations with carbon dioxide inhibition were also reported by Ledakowicz et al. [10], Nettelhoff et al. [11], and Deckwer et al. [12]. As a result, the site balances for the FT catalytic sites read:

$$\theta_{s_1} + (\theta_{Cs_1} \text{ or } \theta_{COs_1}) + \theta_{CO_2 s_1} = 1 \tag{6.1}$$

$$(\theta_{Cs_1} \text{ or } \theta_{COs_1}) + \theta_{CO_2 s_1} = 1 \tag{6.2}$$

with θ_{Cs_1} relevant for dissociative and θ_{COs_1} relevant for associative CO adsorption, respectively.

The final form of the kinetic equations is presented in Table 6.6. These equations were optimized with both site balances (eqs 6.1-6.2). The relative variances of these optimizations and the appropriate ranking are shown in Table 6.7. The statistical significance of the differences in accuracy was tested with Bartlett's test (Chapter 3) [13]. For a number of competitive models H, the Bartlett's test compares a critical calculated χ_c^2 value (for details, see Chapter 3 or Jonker et al. [13]) with a tabulated χ_t^2 value [14]. If χ_c^2 exceeds the tabulated value, the model with the largest deviation was rejected and χ_c^2 was recalculated. Models were subsequently rejected, until χ_c^2 was below the tabulated value. Table 6.8 compares χ_c^2 with the tabulated χ_t^2 value for $H-1$ degrees of freedom. The table shows that the best two models ($H = 2$) passed the test and are statistically indistinguishable. These best models are, in succeeding order: FT-I3 (eq 6.1) and FT-III2 (eq 6.2). Table 6.9 shows the optimized model parameters. The 95 % confidence limits show that the adsorption constant of CO_2 is rather inaccurate. The adsorption constant of CO (a) for model FT-I3 is not significantly different from zero. Therefore, we prefer model FT-III2 for the description of the FT reaction rate. This model is also one of the optimal kinetic equations of the gas-solid system (Chapter 5). Parity graphs of the FT kinetic equations are shown in Figure 6.4.

Based on the formate mechanism and the assumptions mentioned in Chapter 5, two kinetic rate equations for the water gas shift reaction are possible. The expressions are

Table 6.6 Reaction rate expressions considered for the Fischer-Tropsch synthesis, R_{FT} (mol kg_{cat}^{-1} s^{-1}).

Model[1]	Kinetic equation
FT-I3	$\frac{k P_{CO}^{1/2} P_{H_2}^{1/2}}{\left(1 + a P_{CO}^{1/2} + b P_{CO_2}\right)^2}$
FT-I4	$\frac{k P_{CO}^{1/2} P_{H_2}^{3/4}}{\left(1 + a P_{CO}^{1/2} P_{H_2}^{-1/4} + b P_{CO_2}\right)^2}$
FT-II3	$\frac{k P_{CO}^{1/2} P_{H_2}}{1 + a P_{CO}^{1/2} + b P_{CO_2}}$
FT-III2	$\frac{k P_{CO} P_{H_2}^{1/2}}{\left(1 + a P_{CO} + b P_{CO_2}\right)^2}$
FT-III3	$\frac{k P_{CO} P_{H_2}}{\left(1 + a P_{CO} + b P_{CO_2}\right)^2}$
FT-IV2	$\frac{k P_{CO} P_{H_2}}{1 + a P_{CO} + b P_{CO_2}}$
FT-IV3	$\frac{k P_{CO} P_{H_2}^2}{1 + a P_{CO} + b P_{CO_2}}$

[1] See Chapter 5 for a description of these models.

Table 6.7 FT kinetic model screening.

Model	Site balance (eq)	s_{rel} (%)	Rank
FT-I3	6.1	12.9	1
FT-I3	6.2	29.5	6
FT-I4	6.2	27.3	4
FT-II3	6.2	29.2	5
FT-III2	6.1	13.3	2
FT-III2	6.2	32.3	7
FT-III3	6.2	42.5	9
FT-IV2	6.2	25.0	3
FT-IV3	6.2	41.8	8

FT-I4, FT-II3, FT-III2, FTIII3, FT-IV2, FT-IV3 with site balance 6.1 results in $a < 0$ or $b < 0$

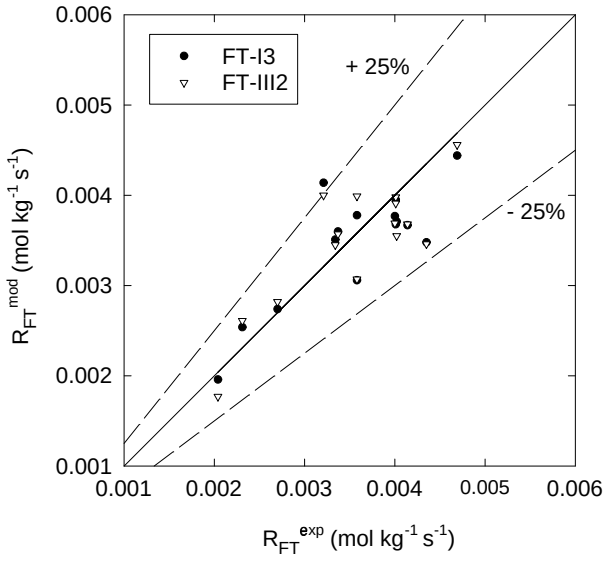

Figure 6.4 Parity graph of the best FT rate equations.

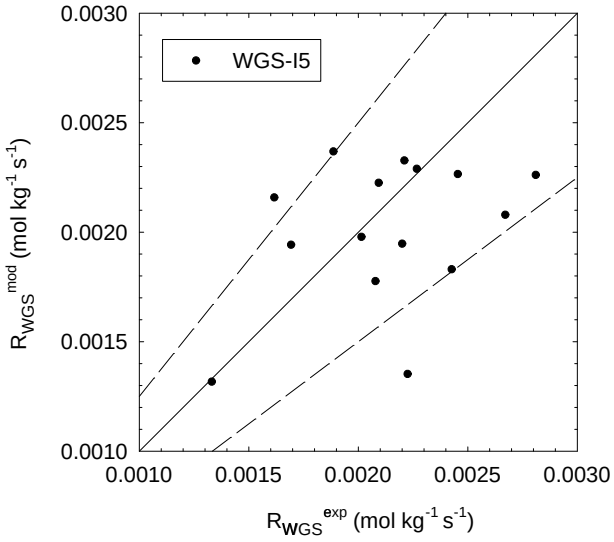

Figure 6.5 Parity graph of the WGS rate equation.

Table 6.8 Bartlett's test for FT models[1].

H	χ_c^2	χ_t^2
9	37.6	15.5
8	31.4	14.1
7	22.0	12.6
6	17.9	11.1
5	13.9	9.49
4	10.7	7.81
3	7.24	5.99
2	0.0107	3.84

[1] χ_c^2: critical χ^2 according to Bartlett's test [13]; χ_t^2: tabulated χ^2 [14]

given in Chapter 5 (Table 5.7). The adsorption of both H_2 and CO_2 is assumed to be negligible relative to CO and H_2O [15–17]. Thus, the mass balance of the catalytic sites, s_2, is:

$$\theta_{s_2} + \theta_{H_2Os_2} + \theta_{COs_2} = 1 \tag{6.3}$$

$$\theta_{H_2Os_2} + \theta_{COs_2} = 1 \tag{6.4}$$

For the temperature dependency of the equilibrium constant of the WGS reaction, K_P, the following relation was used (Graaf et al. [18]):

$$\log K_P = \log\left(\frac{P_{CO_2}P_{H_2}}{P_{H_2O}P_{CO}}\right)_{eq} = \left(\frac{2073}{T} - 2.029\right) \tag{6.5}$$

The agreement between the experiments and the kinetic models is not impressive. Model WGS-I5 with site balance eq. 6.4 fitted the experimental rates the best (s_{rel}= 20.5 %).

$$R_{WGS-I5} = \frac{k_w/K_1^2\left(P_{CO}P_{H_2O} - P_{CO_2}P_{H_2}/K_P\right)}{\left(P_{CO} + \frac{K_3}{K_1}P_{H_2O}\right)^2} \tag{6.6}$$

The relative variance of the other kinetic models exceeded 30 % or the values of the optimized parameters were unrealistic. The corresponding model parameters are given in Table 6.9 and the parity graph is shown in Figure 6.5.

Table 6.9 Final estimates of the parameters of the FT and WGS kinetic models.

Parameter	Dimension	Estimate
FT-I3 (s_{rel} 12.9 %)		
k	mol kg^{-1} s^{-1} MPa$^{-1.25}$	0.011 ± 0.004
a	MPa^{-1}	0.175 ± 0.204
b	MPa^{-1}	0.485 ± 0.365
FT-III2 (s_{rel} 13.3 %)		
k	mol kg^{-1} s^{-1} MPa$^{-1.5}$	0.034 ± 0.011
a	MPa^{-1}	1.185 ± 0.357
b	MPa^{-1}	0.656 ± 0.456
WGS-I5 (s_{rel} 20.5 %)		
k_w/K_1^2	mol kg^{-1} s^{-1}	0.030 ± 0.003
K_3/K_1	-	3.07 ± 0.31

A comparison between the experimental and the calculated reaction rates of the Fischer-Tropsch and the water gas shift reaction is presented in Figure 6.6a-b. The calculated rates are based on the optimal kinetic models FT-III2 and WGS-I5. The behavior of the kinetic reactor was calculated with a CSTR model (see Chapter 5 for details). Figure 6.6a shows the effect of the flow rate on the overall synthesis gas consumption rate and on reaction rates of the both Fischer-Tropsch reaction and the water gas shift reaction. There appears to be good agreement between the experimental and the calculated reaction rates over the measured range of space velocity. The reaction rates increase with increasing space velocity due to decreasing inhibitor concentrations (FT: CO_2; WGS: H_2O).

The effect of the feed ratio of H_2/CO at a constant reactor pressure of 1.5 MPa is shown in Figure 6.6b. Both the Fischer-Tropsch and the water gas shift reaction rate decrease slightly towards lower H_2/CO ratios. The overall synthesis gas consumption rate decreases strongly due to the reaction stoichiometry. Figure 6.6b also compares the reaction rates observed with the gas-slurry system and in the gas-solid system (Chapter 5). The model lines for the gas-solid system were calculated at comparable conditions with the optimal kinetic equations: FT-III2 and WGS-I6 (Chapter 5; see Table 5.10). At high feed ratios ($F > 2$), the reaction rates in the gas-slurry and the gas-solid systems are nearly the same. However, at low H_2/CO ratios, the reaction rates in the gas-solid system are significantly higher than in the gas-slurry system. The main difference between the reaction rate equations for two systems is in the inhibitor

term. Both optimal models for the gas-slurry system contain CO_2 inhibition in contrast to H_2O inhibition for the gas-solid system, see Chapter 5. Consequently, the gas-slurry reaction rates are inhibited at low H_2/CO ratios due to CO_2 formed via the water gas shift reaction. The water gas shift reaction is rather slow in the slurry phase relative to the gas-solid system. In case of the gas-slurry system, the WGS catalytic sites are completely covered. Apparently, the presence of the liquid phase affects the adsorption strength of the components present.

6.4 Conclusions

- The product selectivity model ORPDM, previously developed to describe gas-solid selectivity, also appears to describe accurately the selectivities over a precipitated iron catalyst in the slurry phase. The average deviation of the selectivity to paraffins and olefins is 10.6 % and 8.7 %, respectively.

- The presence of the slurry liquid appears to affect the product selectivity relative to the gas-solid system. The slurry-phase system yields a higher olefin fraction at comparable reaction conditions. The corresponding model parameters, the readsorption constant and the termination constant to olefins, are lower at similar conditions.

- The reaction kinetics of both the Fischer-Tropsch and the water gas shift reaction in the gas-slurry system can be described with the same set of reaction mechanisms found previously to describe the gas-solid system. The reaction rates appear to be comparable at high H_2/CO feed ratios. However, the reaction rate of the FT synthesis appears to be lower at H_2/CO ratios below 2 due to inhibition of CO_2 in the slurry system. The water gas shift reaction rate is also lower at these low H_2/CO ratios due to complete occupation of the WGS catalytic sites.

References

[1] Saxena, S.C.; Rosen, M.; Smith, D.N.; Ruether, J.A., Mathematical modeling of Fischer-Tropsch slurry bubble column reactors, *Chem. Eng. Commun.* **1986**, *40*, 97–151.

[2] Van der Laan, G.P.; Beenackers, A.A.C.M.; Ding, B.; Strikwerda, J.C., Liquid-

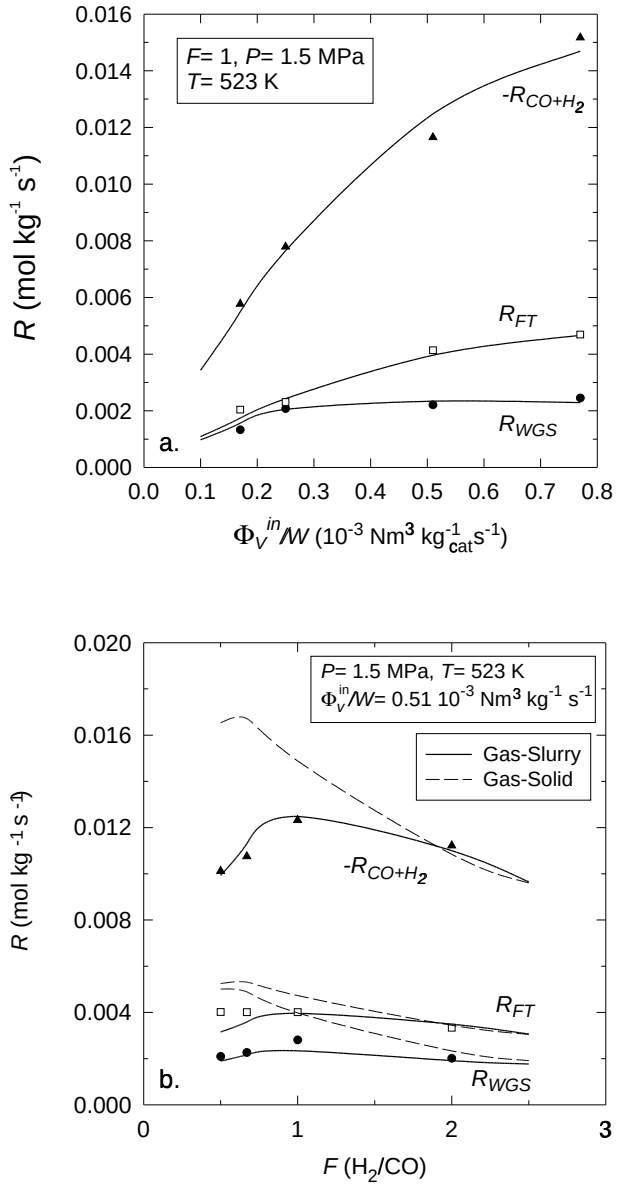

Figure 6.6 Reaction rates for the FT, WGS, and total conversion of CO and H_2 versus space velocity (a) and feed ratio H_2/CO (b). Dotted lines are model predictions of the optimal kinetic equations for the gas-solid system (FT-III2 and WGS-II6, see Chapter 5). Symbols are experimental values. Solid lines are model predictions (FT-III2 and WGS-I5).

phase methanol synthesis in apolar (squalane) and polar (tetraethylene glycol dimethylether) solvents, *Catal. Today* **1999**, *48*, 93–100.

[3] Stenger, H.G.; Satterfield, C.N., Effect of liquid composition on the slurry Fischer-Tropsch synthesis. 1. Rate of reaction, *Ind. Eng. Chem. Process Des. Dev.* **1985**, *24*, 407–411.

[4] Stenger, H.G.; Satterfield, C.N., Effect of liquid composition on the slurry Fischer-Tropsch synthesis. 2. Product selectivity, *Ind. Eng. Chem. Process Des. Dev.* **1985**, *24*, 411–415.

[5] Bukur, D.B.; Patel, S.A.; Lang, X., Fixed bed and slurry reactor studies of Fischer-Tropsch synthesis on precipitated iron catalyst, *Appl. Catal. A* **1990**, *61*, 329–349.

[6] Graaf, G.H.; Winkelman, J.G.M.; Stamhuis, E.J.; Beenackers, A.A.C.M., Kinetics of the three-phase methanol synthesis, *Chem. Eng. Sci.* **1988**, *43*, 2161–2168.

[7] Breman, B.B.; Beenackers, A.A.C.M.; Schuurman, H.A.; Oesterholt, E., Kinetics of the gas-slurry methanol-higher alcohol synthesis from $CO/CO_2/H_2$ over a $Cs\text{-}Cu/ZnO/Al_2O_3$ catalyst, including simultaneous formation of methyl esters and hydrocarbons, *Catal. Today* **1995**, *24*, 5–14.

[8] Bukur, D.B.; Nowicki, L.; Manne, R.K.; Lang, X., Activation studies with a precipitated iron catalyst for Fischer-Tropsch synthesis 2. Reaction studies, *J. Catal.* **1995**, *155*, 366–375.

[9] Press, W.H.; Flannery, B.P.; Teukolsky, S.A.; Vetterling, W.T., *Numerical recipes in Pascal*, Cambridge University Press, New York **1989**.

[10] Ledakowicz, S.; Nettelhoff, H.; Kokuun, R.; Deckwer, W.-D., Kinetics of the Fischer-Tropsch synthesis in the slurry phase on a potassium-promoted iron catalyst, *Top. Catal.* **1985**, *24*, 1043–1049.

[11] Nettelhoff, H.; Kokuun, R.; Ledakowicz, S.; Deckwer, W.-D., Studies on the kinetics of Fischer-Tropsch synthesis in slurry phase, *Ger. Chem. Eng.* **1985**, *8*, 177–185.

[12] Deckwer, W.-D.; Kokuun, R.; Sanders, E.; Ledakowicz, S., Kinetic studies of Fischer-Tropsch synthesis on suspended Fe/K catalyst. Rate inhibition by CO_2 and H_2O, *Ind. Eng. Chem. Process Des. Dev.* **1986**, *25*, 643–649.

[13] Jonker, G.H.; Veldsink, J.-W.; Beenackers, A.A.C.M., Intrinsic kinetics of 9-monoenic fatty acid methyl ester hydrogenation over nickel-based catalysts, *Ind. Eng. Chem. Res.* **1997**, *36*, 1567–1579.

[14] Fisher, R.A, *Statistical methods for research workers*, Macmillan, 14th edn. **1970**.

[15] Dry, M.E.; Shingles, T.; Boshoff, L.J.; Oosthuizen, G.J., Heats of adsorption on promoted iron surfaces and the role of alkali in Fischer-Tropsch synthesis, *J. Catal.* **1969**, *15*, 190–199.

[16] Zimmerman, W.H.; Bukur, D.B., Reaction kinetics over iron catalysts used for the Fischer-Tropsch synthesis, *Can. J. Chem. Eng.* **1990**, *68*, 292–301.

[17] Lox, E.S.; Froment, G.F., Kinetics of the Fischer-Tropsch reaction on a precipitated promoted iron catalyst. 2. Kinetic modeling, *Ind. Eng. Chem. Res.* **1993**, *32*, 71–82.

[18] Graaf, G.H.; Sijtsema, P.J.J.M.; Stamhuis, E.J.; Joosten, G.E.H., Chemical equilibria in methanol synthesis, *Chem. Eng. Sci.* **1986**, *41*, 2883–2890.